Title: Brownian Dynamics Simulation of the Aggregation of Submicron Particles in Static Gas

Author: Mariko Watanabe Daisuke Tanaka

PII: S0098-1354(13)00093-8
DOI: http://dx.doi.org/doi:10.1016/j.compchemeng.2013.03.028
Reference: CACE 4685

To appear in: *Computers and Chemical Engineering*

Received date: 27-7-2011
Revised date: 11-3-2013
Accepted date: 26-3-2013

Please cite this article as: Watanabe, M., & Tanaka, D., Brownian Dynamics Simulation of the Aggregation of Submicron Particles in Static Gas, *Computers and Chemical Engineering* (2013), http://dx.doi.org/10.1016/j.compchemeng.2013.03.028

Brownian Dynamics Simulation of the Aggregation of Submicron Particles in Static Gas

Mariko Watanabe[1)], Daisuke Tanaka[2)]

[1)] *Department of Engineering and Applied Sciences, Sophia University, 7-1 Kioi-cho, Chiyoda-ku, Tokyo 102-8554, Japan*

[2)] *Department of Mechanical Engineering, Osaka University, 2-1 Yamadaoka, Suita, Osaka 565-0871, Japan*

ABSTRACT

A Brownian dynamics simulation was conducted to investigate the formation of aggregates that are composed of submicron particles such as soot. Three models were considered for aggregation: a diffusion-limited aggregation model, in which an aggregate grows around a fixed particle; a particle–cluster aggregation model, in which a single aggregate grows by collisions between particles and the aggregate; and a cluster–cluster aggregation (CCA) model, in which many particles and aggregates form multiple aggregates. A comparison of the three aggregation models showed that the CCA model resulted in a soot-like branching shape. The aggregation was investigated by employing the CCA model; it was determined that increase in gas temperature affected the shielding effect of the aggregate branch by changing the displacement and velocity of Brownian particles. Furthermore, these simulations demonstrated that the size and aspect ratio of the field and the particle density also affected aggregation shape.

Key Words: Brownian Dynamics Simulation, Aggregation, Submicron Particle

[1)] Corresponding author Department of Engineering and Applied Sciences, Sophia University, 7-1 Kioi-cho, Chiyoda-ku, Tokyo 102-8554, Japan
E-mail: mariko_w@sophia.ac.jp TEL&FAX: 81-3-3238-3606

1. Introduction

After-treatment technologies, such as diesel particulate filters (DPFs), remove soot that is emitted from diesel engines and are an important means of dealing with residual soot that cannot be eliminated by refining the combustion process. Since pressure loss by DPFs causes a drop in engine power, DPFs need a high adsorption efficiency that can help minimize the pressure loss. Furthermore, DPFs demand a long regeneration cycle, affecting fuel efficiency. For optimal performance, DPFs need to capture soot uniformly.

Improving DPF performance requires an understanding of the motion and agglomeration of soot particles. In 2007, Ohara et al. directly measured particles that are released in the exhaust of a diesel engine after passing through a DPF. However, it is often difficult to obtain empirical time-series data of soot particle behavior, because primary soot particles are tens of nanometers in diameter, whereas the aggregates of primary soot particles that[Editor1] come together to form secondary particles are several micrometers in diameter. To address this difficulty, some researchers have conducted numerical simulations of soot particle motion and their resultant aggregation on a wall. Sbrizzai et al. (2005) and Bensaid et al. (2009, 2010) calculated the flow in a microchannel and a porous wall of a DPF by computational fluid dynamics to investigate particle motion and their deposition position. Similarly, Yamamoto et al. (2009) simulated the flow through a porous filter, whose detailed structure was obtained by utilizing three-dimensional CT images. Furthermore, Hayashi and Kubo (2008) conducted a numerical simulation of the filtration of soot particles in a DPF by the lattice Boltzmann method for gas and the Brownian dynamics method for suspended soot particles. However, almost all these studies calculated either a single

soot particle individually or soot concentration and ignored the shape of the aggregated soot particles.

To account for the effects of soot structure, the following studies include a simulated Brownian force. Brownian force is random and acts on submicron particles such as soot. Various calculations that consider Brownian diffusion have been investigated to determine aggregate formation and structure (Kempf et al., 1999; Brasil et al., 2001; Paszun and Dominik, 2006). However, these investigations have largely been oversimplifications, and a Langevin equation of Brownian particles that accounts for aggregate translation and rotation as well as for momentum exchange when particle–particle, particle–aggregate, or aggregate–aggregate collisions occur has not been solved simultaneously. Therefore, this study conducts a Brownian dynamics simulation that considers aggregate motion, collision, and agglomeration and investigates the effects of gas temperature and boundary on the shape of aggregates.

2. Calculation method

2.1 Langevin equation

The Langevin equation is a motion equation that is applicable to Brownian particles. In this equation, random motion caused by collisions between a particle and fluid molecules is expressed as the Brownian force that is generated by utilizing random numbers. The Langevin equation is expressed as (Ermak and Buckholz, 1980)

$$m\frac{d\mathbf{v}}{dt} = m\mathbf{g} - \frac{m\zeta}{\mathrm{C_C}}\mathbf{v} + \mathbf{F}^{\mathrm{B}}, \tag{1}$$

$$\mathrm{C_C} = 1 + \mathrm{Kn}\left\{1.142 + 0.058\exp\left(-0.999/\mathrm{Kn}\right)\right\}, \tag{2}$$

where m is the particle mass, $\mathbf{v}$ is the particle velocity, $\mathbf{g}$ is gravity, $m\zeta$ is the friction

coefficient, Kn is the Knudsen number, and Cc is the Cunningham correction factor. It is assumed that the particle is a sphere and that drag acts on the particle according to Stokes' law. The friction coefficient is given as

$$m\zeta = 6\pi\mu a\,, \tag{3}$$

where a is the particle radius, and μ is the gas viscosity. The Brownian force, $\mathbf{F}^{\mathrm{B}}$, satisfies the following equations when k is the Boltzmann constant, T is the temperature, δ is the Dirac δ function, and the angle brackets show the mean value:

$$\left\langle \mathbf{F}^{\mathrm{B}} \right\rangle = 0\,, \tag{4}$$

$$\left\langle \mathbf{F}^{\mathrm{B}}(t) \bullet \mathbf{F}^{\mathrm{B}}(t') \right\rangle = 6m\zeta^{*}kT\delta(t-t')\,, \tag{5}$$

where $\zeta^{*} = \zeta/\mathrm{C_C}$.

When a time step, δt, is sufficiently longer than the relaxation time of the momentum of Brownian particles, ($t_{relax} = 1/\zeta^{*} = m\mathrm{C_C}/6\pi\mu a$), yet sufficiently small to be regarded as a constant external force acting on particles, the following equations of displacement and velocity of the particles are obtained by integrating eq.(1):

$$\begin{aligned}\mathbf{r}(t+\delta t) = \mathbf{r}(t) + \frac{1}{\zeta^{*}}\mathbf{v}(t)\left\{1-\exp\left(-\zeta^{*}\delta t\right)\right\} + \delta\mathbf{r}^{B}(t+\delta t) \\ + \frac{1}{m\zeta^{*}}\mathbf{F}(t)\left[\delta t - \frac{1}{\zeta^{*}}\left\{1-\exp\left(-\zeta^{*}\delta t\right)\right\}\right]\end{aligned}\,, \tag{6}$$

$$\mathbf{v}(t+\delta t) = \mathbf{v}(t)\exp\left(-\zeta^{*}\delta t\right) + \delta\mathbf{v}^{B}(t+\delta t) + \frac{1}{m\zeta^{*}}\mathbf{F}(t)\left\{1-\exp\left(-\zeta^{*}\delta t\right)\right\}. \tag{7}$$

The random displacement and velocity, $\delta\mathbf{r}^{\mathrm{B}}$ and $\delta\mathbf{v}^{\mathrm{B}}$, respectively, satisfy the following statistical characteristics:

$$\left\langle \delta\mathbf{r}^{B} \right\rangle = \left\langle \delta\mathbf{v}^{B} \right\rangle = 0\,, \tag{8a}$$

$$\left\langle \delta\mathbf{r}^{B} \cdot \delta\mathbf{v}^{B} \right\rangle = 3H\,, \tag{8b}$$

$$\left\langle \left(\delta \mathbf{r}^{B}\right)^{2} \right\rangle = 3G\,, \tag{8c}$$

$$\left\langle \left(\delta \mathbf{v}^{B}\right)^{2} \right\rangle = 3E\,, \tag{8d}$$

where

$$E = \frac{kT}{m\zeta^{*2}}\left\{2\zeta^{*}\delta t - 3 + 4\exp\left(-\zeta^{*}\delta t\right) - \exp\left(-2\zeta^{*}\delta t\right)\right\}, \tag{9a}$$

$$G = \frac{kT}{m}\left\{1 - \exp\left(-2\zeta^{*}\delta t\right)\right\}, \text{ and} \tag{9b}$$

$$H = \frac{kT}{m\zeta^{*}}\left\{1 - \exp\left(-\zeta^{*}\delta t\right)\right\}^{2}. \tag{9c}$$

When the Cartesian coordinate system (x, y, z) is considered, the x-direction random displacement and velocity, δx^{B} and δv_x^B, respectively,[Editor2] are calculated by the Box–Muller method as follows:

$$\delta v_x^B = \left(-2\sigma_v^2 \ln R_1\right)^{1/2} \cos 2\pi R_2\,, \tag{10a}$$

$$\delta x^B = c_{rv}\frac{\sigma_r}{\sigma_v}\delta v_x^B + \left(1 - c_{rv}^2\right)^{1/2}\left(-2\sigma_r^2 \ln R_3\right)^{1/2} \cos 2\pi R_4\,, \tag{10b}$$

where R_1, R_2, R_3, R_4 are uniform random numbers. In this study, the Mersenne twister (MT19937) was employed as a random number generator. Here σ_r, σ_v, c_{rv} are given as follows:

$$\sigma_r^2 = E = \frac{kT}{m\zeta^{*2}}\left\{2\zeta^{*}\delta t - 3 + 4\exp\left(-\zeta^{*}\delta t\right) - \exp\left(-2\zeta^{*}\delta t\right)\right\}, \tag{11a}$$

$$\sigma_v^2 = G = \frac{kT}{m}\left\{1 - \exp\left(-2\zeta^{*}\delta t\right)\right\}, \tag{11b}$$

$$c_{rv} = \frac{H}{(EG)^{1/2}} = \frac{1}{\sigma_r \sigma_v} \cdot \frac{kT}{m\zeta^*} \left\{1 - \exp\left(-\zeta^* \delta t\right)\right\}^2, \tag{11c}$$

where c_{rv} is a constant that satisfies the condition $-1 < c_{rv} < 1$.

The random walk of a Brownian particle can also be obtained by calculating random force rather than random displacement and velocity. In the Brownian dynamics simulation, the acceleration term $m d\mathbf{v}/dt$ is negligible, because the time step is sufficiently larger than the momentum relaxation time. Therefore, the motion equation of a particle is expressed as follows:

$$m\mathbf{g} - \frac{m\zeta}{\mathrm{C_C}}\mathbf{v} + \mathbf{F}^B = 0. \tag{12}$$

The velocity of a Brownian particle is expressed as

$$\mathbf{v} = \frac{\mathrm{C_C}}{m\zeta}\left(\mathbf{F}^B + m\mathbf{g}\right). \tag{13}$$

When gas flows with velocity **U**, the Brownian particle velocity is obtained as

$$\mathbf{v} = \frac{\mathrm{C_C}}{m\zeta}\left(\mathbf{F}^B + m\mathbf{g}\right) + \mathbf{U}. \tag{14}$$

The random force is expressed by the Box–Muller method when the uniform random numbers are R_1 and R_2, and it is given as

$$\mathbf{F}^B = \left(-2\sigma^2 \ln R_1\right)^{1/2} \cos 2\pi R_2, \tag{15}$$

where σ^2 is variance given by $\sigma^2 = 2m\zeta kT/\delta t$.

2.2 Motion equation of aggregate

The translational velocity of an aggregate, **V**, is expressed as

$$\mathbf{V} = \frac{\mathrm{C_C}}{M\zeta}\left(\mathbf{F}_{agg}^{B} + M\mathbf{g}\right) + \mathbf{U}\,, \tag{16}$$

$$M = \sum_{i=1}^{N_p} m_i\,, \tag{17a}$$

$$M\zeta = 6\pi\mu a_{rms}\,, \tag{17b}$$

$$a_{rms} = \sqrt{\frac{1}{N_p}\sum_{i=1}^{N_p} r_i^2}\,, \text{ and} \tag{17c}$$

$$\mathbf{F}_{agg}^{B} = \sum_{i=1}^{N_p} \mathbf{F}_i^{B}\,, \tag{17d}$$

where the subscript i indicates the i-th particle, M is the mass of the aggregate, N_p is the total number of particles including the aggregate, a_{rms} is the square mean value of r_i, r_i is the distance from the center of gravity of the aggregate to the i-th constituent particle, and $\mathbf{F}_{agg}^{B}$ is the Brownian force that acts on the aggregate. The Cunningham correction term is calculated by utilizing a_{rms}. A few studies have proposed a model for the friction coefficient between aggregates and fluid (Doi and Chen, 1989; Higashitani et al., 2001). However, a practical model of the hydrodynamic drag force of an aggregate with any arrangement of particles has not been established. Meanwhile, the calculation of the interaction between aggregates and fluid, which considers in detail any arrangement of particles in the cluster, imposes a high calculation cost. Accordingly, aggregates are approximated as spheres when the friction coefficient of an aggregate is calculated in this study.

To describe the rotational motion of aggregates, a coordinate that is fixed on the aggregate and whose origin agrees with the center of gravity of the aggregate is used. In this study, a coordinate fixed in space is called a spatial coordinate system ($O-xyz$) and

a coordinate fixed in an aggregate is called an aggregate coordinate system ($G-\tilde{x}\tilde{y}\tilde{z}$) (Fig.1). The three axes of the aggregate coordinate system are chosen so that they agree with the main inertia axes. When O agrees with G and Euler angles (θ,ϕ,ψ) are set as shown in Fig.2, the transformation matrix, **R**, from $O-xyz$ to $G-\tilde{x}\tilde{y}\tilde{z}$ is expressed as follows:

$$\mathbf{R}=\begin{pmatrix} \cos\psi\cos\phi-\cos\theta\sin\phi\sin\psi & \cos\psi\sin\phi+\cos\theta\cos\phi\sin\psi & \sin\psi\sin\theta \\ -\sin\psi\cos\phi-\cos\theta\sin\phi\cos\psi & -\sin\psi\sin\phi+\cos\theta\cos\phi\cos\psi & \cos\psi\sin\theta \\ \sin\theta\sin\phi & -\sin\theta\cos\phi & \cos\theta \end{pmatrix}. \quad (18)$$

Similar to the translation motion equation, the angular acceleration of an aggregate is negligible. Therefore, the angular velocity is expressed as

$$\boldsymbol{\omega}=\frac{\mathrm{C_C}}{8\pi\mu a_{rms}^3}\mathbf{T}_R^{\mathrm{B}}+\boldsymbol{\Omega}, \quad (19)$$

where $\boldsymbol{\Omega}$ is the flow angular velocity vector on the aggregate-coordinate system, and $\mathbf{T}_R^{\mathrm{B}}$ is the Brownian torque given as

$$\mathbf{T}_R^{\mathrm{B}}=\mathbf{R}\left(\sum_i \mathbf{r}_i'\times\mathbf{F}_i^B\right), \quad (20)$$

where $\mathbf{r}_i'$ is the relative displacement vector of the constituent particle from the center of gravity on the spatial coordinate system.

2.3 Aggregation models

This study uses three aggregation models. Schematics of these models are shown in Fig.3. In all the models, the colliding particles or aggregates are frozen when they first touch and do not overlap. All particles and aggregates are treated as rigid bodies. It is assumed that there is no destruction of aggregates.

2.3.1 Diffusion-Limited Aggregation (DLA) model

A DLA model is a pattern-growth model for a non-equilibrium condition. The algorithm is as follows:

1. A seed particle is fixed at the origin.

2. A particle is fixed at a random point at some distance from the origin.

3. The particle's random velocity and displacement are calculated and its position and velocity are decided from the Langevin equation.

4. When the particle touches the seed particle of the aggregate, the particle stops and becomes a part of the aggregate.

Steps 2, 3, and 4 are repeated, and the aggregate grows.

2.3.2 Particle–Cluster Aggregation (PCA) model and Cluster–Cluster Aggregation (CCA) model

In the PCA model, many particles exist in a space and move simultaneously. Initially, two particles collide to form an aggregate as a result of a perfectly inelastic collision. It is assumed that only one aggregate is formed and it increased in size. Perfectly inelastic collisions occur when particles collide with the aggregate. When particles collide with other particles, perfectly elastic collisions occur.

In the CCA model, many particles exist in a space and move simultaneously, as in the PCA model. However, in this model, all collisions are perfectly inelastic. As a result, several aggregates are formed, and collisions among multiple aggregates occur. The algorithm of both the models is as follows:

1. The initial velocity of all single particles and the translational and rotational velocities of all aggregates are calculated by eqs. (14), (16), and (19).

2. When the first collision occurs before the next Brownian force acts, all particles and aggregates move until the first collision occurs.

3. In the PCA model, the new velocity is calculated on the basis of a perfectly inelastic collision for collision between a particle and the aggregate and a perfectly elastic collision for all other collisions. In the CCA model, the new velocity is calculated on the basis of a perfectly inelastic collision in all cases.

4. Steps 2 and 3 are repeated until the next collision occurs after the next Brownian force acts.

5. If the predicted time of the next collision is longer than the time when the next Brownian force acts, all particles and aggregates move until the next Brownian force acts, and the calculation returns to step 1. Then, a new velocity is calculated.

2.4 Calculation condition

Particle motion for the DLA model was calculated by utilizing eqs. (6) and (7). For the PCA and CCA models, eq. (14) was utilized as the particle motion equation. The selected Knudsen number was 1.36 on the basis of the particle radius and mean free path of air at atmospheric condition. The ratio of particles to fluid was 7.72×10^2. The fluid viscosity was measured at atmospheric pressure and at 473, 573, and 873 K. The number of particles in the calculation area was 500. The time step with the DLA model was 1.0×10^{-5} s, and with PCA and CCA models, it was 1.0×10^{-6} s. The three forces acting on the particles were Brownian force, gravity, and drag based on Stoke's law. The probability density distributions of random displacement and velocity for the DLA model and those of random force for PCA and CCA models are shown in Fig.4. With increase in fluid temperature, the width of each distribution extends, and the peak

decreases. The calculation was conducted 26 times for the DLA model and 20 times for PCA and CCA models. The results were averaged.

3. Results and Discussion

3.1 Comparison of the aggregation model

For PCA and CCA models, the calculation area was an $80D$ ($D = 2a$) cube with a periodic boundary condition in all directions. Figure 5 shows an example of the aggregate obtained by the three aggregation models: (a) DLA; (b) PCA; and (c) CCA. Figure 6 shows the fractal dimension of the aggregates obtained by each model. The fractal dimension, D_f, is defined as

$$N_p = B\left(\frac{a_{rms}}{a}\right)^{D_f}, \tag{21}$$

$$B = \frac{\alpha_s}{\alpha_v}, \tag{22}$$

where B is the fractal pre-factor, α_s is the surface shape factor, and α_v is the volume shape factor. The D_f of a sphere and disc are 3 and 2, respectively. Many of the aggregates have a D_f in the range of 1.5–2.5 (Koylu et al., 1995; Brasil et al., 2001; Sorensen, 2001).

DLA and PCA models give aggregates with similar shape and D_f, because the algorithm by which the particle approaches and agglomerates is common to both models. However, the D_f obtained from the PCA model is greater than that obtained from the DLA model, because the aggregate grows around its center of gravity in the PCA model and around a fixed seed particle in the DLA model. Thus, the relative velocity between the aggregate and particles differs between the PCA model and the DLA model, because

the former model allows for aggregate translation and rotation. Therefore, the shielding effect changes, and the branches of the aggregate interrupt the entrance of additional particles. The CCA model gives a soot-like branching aggregate (see Fig. 7). In this model, the aggregate shape differs from that in the other two models, because many aggregates are formed and increase in size as a result of collisions between aggregates. Because the orientation of the aggregates before collision affects aggregate shape in the CCA model, the aggregate grows more randomly in this model than in the other two models.

Utilizing the DLA and CCA models, the highest D_f was obtained at 573 K. The Brownian motion of particles and aggregates changes with changes in temperature. The displacement of particles is small at lower temperatures and increases as temperature increases. Because particles remain close to the aggregate at lower temperatures, the probability with which the particle will adhere to a branch of the aggregate increases. On the other hand, the particle will easily collide with a branch of the aggregate when the displacement is large. It seems that the particles are not affected by the shielding effect at 573 K and they move with displacement. In contrast, in the PCA model, the D_f barely changes with changes in temperature, because the relative velocity of the particle and aggregate is large in comparison to the negligible changes in the Brownian motion caused by temperature fluctuations.

3.2 Aggregation in static cubic area

Aggregation in static gas was investigated by the CCA model with a reflection boundary in all directions. The calculation area was a cube with varying dimensions, with sides of 20, 30, 40, 60, and 80*D*. The number of particles was constant, allowing

comparison of the final shape of the aggregate. The number density was varied by changing the calculation area size.

Figures 8 and 9 show examples of the aggregates and spatial distribution of a number of particles at 473 K. In Fig. 9, the horizontal axis shows the distance from the center of gravity of the aggregate normalized by D, and the vertical axis shows a number of particles included in the spherical shell located at a distance. The height and position of the peak indicate the compactness of the aggregates. The width of the distribution relates to aggregate size and length of branches. The width of the distribution expands, and the peak becomes small and shifts to the right, as the area size increases in Fig.9. It is found that the aggregate becomes branching as the calculation area expands from Figs. 8 and 9. Figure 10 shows the fractal dimension of the aggregates formed in each calculation area. The fractal dimension decreases as the calculation area expands. The shape and fractal dimension change only slightly in a large calculation area. Although the fractal dimension barely changes between $60D$ and $80D$, the fractal dimensions of the resultant particle when the area size is $80D$ and has a periodic boundary in all directions, which are D_f = 1.25 at 473 K, D_f = 1.28 at 573 K, and D_f = 1.25 at 873 K, are smaller than those at $80D$. This is because while the aggregate orientation is parallel to the wall at a reflection, the aggregate orientation is free at a periodic boundary, allowing the branch of the aggregate to grow easily. Similarly, the fractal dimension decreases as the calculation area expands. When the calculation area is small, the particles are crowded, and their orientations are restricted by the reflection wall.

At $20D$, changes in temperature have a marginal effect on D_f, because the area size is small, and particles are crowded. Consequently, the particles collide without any

relationship to changes in displacement and velocity as a result of changes in temperature. The D_f changes with temperature in other area sizes, because both the particle velocity and the shielding effect change with temperature.

3.3 Aggregation in a static rectangular parallelepiped area

Aggregation in a static rectangular parallelepiped area was investigated by the CCA model with a reflection boundary in all directions. The z-direction size of the calculation area was 80*D*, and the x- and y-direction sizes were equal and varied to 20, 30, 40, 60, and 80*D*. The number of particles was maintained constant to compare the final shape of the aggregate. Therefore, the number density, area size, and the aspect ratio of the calculation area changed simultaneously.

Figure 11 shows examples of the aggregates at 473 K. The aggregate increases over the z-direction when the aspect ratio of the calculation area is large and has a branching shape in all directions as the area size increases and the aspect ratio decreases. Figure 12 shows the spatial distribution of a number of particles at 473 K. The distribution shape is relatively flat at 20*D*. The peak becomes large, and the width of the peak decreases as the calculation area expands. This result also indicates that the shape of aggregates changes from a long and narrow shape to a randomly branching shape with expansion in calculation area and decrease in aspect ratio. Figure 13 shows the fractal dimension of the aggregates formed in each calculation area. The fractal dimension is positively correlated with the calculation area at 473 K. This trend agrees with the change in the aggregation shape (Figs. 11 and 12), because the orientation of the aggregate becomes parallel to the wall in a long and narrow area. The fractal dimension is the largest at 873 K, because particles approach the center of the

aggregate positioned parallel to the wall. At lower temperatures, the aggregate rotates while the particles move slowly, making it easier for the particles to adhere to the tip of the aggregate. The change in the fractal dimension with an increase in temperature is large in the 30D space. The wall measuring 30D crowds the aggregates and disturbs their rotation.

4. Conclusion

A Brownian dynamics simulation of the aggregation of submicron particles was conducted. A Langevin equation that included fluid resistance, random force, and gravity was solved.

First, three aggregation models, DLA, PCA, and CCA, were investigated. The comparison demonstrated that although the fractal dimension of the aggregates obtained from the PCA model was slightly larger than that obtained from the DLA model, the shapes of the aggregates were similar. In contrast, a soot-like branching shape was obtained from the CCA model.

Second, aggregate formation in a stationary gas surrounded by reflection boundaries was simulated by the CCA model. Here gas temperature affected the aggregation shape, because the shielding effect of the aggregate branch changed with the probability density distribution of displacement and velocity of Brownian particles due to an increase in the gas temperature. The change in the aggregation shape appeared to depend on area size and particle number density. The particles formed a blocky shape in a small area with high particle number density. In contrast, as the area increased and the particle number density decreased, the branching of the aggregate increased. When the wall was a periodic boundary, the branch grew more freely.

Moreover, the aspect ratio of the calculation area also affected the aggregation shape.

5. Acknowledgments

This research was carried out under the Program of Promotion of Environmental Improvement to Enhance Young Researchers' Independence, the Special Coordination Funds for Promoting Science and Technology, Japan Ministry of Education, Culture, Sports, Science and Technology. This work was supported by KAKENHI (22760129) and Kurata Grants. We thank Prof. Kajishima and Prof. Shibahara of Osaka University for their discussion.

References

Bensaid S, Marchisio DL, Fino D, Saracco G, Specchia V. Modelling of diesel particulate filtration in wall-flow traps. Chemical Engineering Journal 2009; 154: 211–218.

Bensaid S, Marchisio DL, Fino D. Numerical simulation of soot filtration and combustion within diesel particulate filters. Chemical Engineering Science 2010; 65: 357–363.

Brasil AM, Farias TL, Garvalho MG, Koylu UO. Numerical characterization of the morphology of aggregated particles. Journal of Aerosol Science 2001; 32: 489–508.

Doi M, Chen D. Simulation of aggregating colloids in shear flow. The Journal of Chemical Physics 1989; 90: 5271–5279.

Ermak DL, Buckholz H. Numerical integration of the Langevin equation: Monte Carlo simulation. Journal of Computational Physics 1980; 35: 169–182.

Hayashi H, Kubo S. Computer simulation study on filtration of soot particles in diesel particulate filter. Computers and Mathematics with Applications 2008; 55: 1450–1460.

Higashitani K, Iimura K, Sanda H. Simulation of deformation and breakup of large aggregates in flows of viscous fluids. Chemical Engineering Science 2001; 56: 2927–2938.

Ikegami M. Soot formation fundamentals. In: Someya T, editor. Advanced Combustion Science. Tokyo: Springer–Verlag; 1993. p. 165.

Kempf S, Pfalzner S, Henning TK. N-particle-simulations of dust growth. 1. Growth driven by Brownian motion. Icarus 1999; 141: 388–398.

Koylu UO, Xing Y, Rosner DE. Fractal morphology analysis of combustion-generated aggregates using angular light scattering and electron microscope images. Langmuir 1995; 11: 4848–4854.

Ohara E, Mizuno Y, Miyairi Y, Mizutani T, Yuuki K, Noguchi Y, Hiramatsu T, Makino M, Takahashi A, Sasaki H, Tanaka M, Martin A, Fujii S, Busch P, Toyoshima T, Ito T, Lappas I, Vogt CD. Filtration behavior of diesel particulate filters (1). SAE Technical paper 2007; 2007-01-0921.

Paszun D, Dominik C. The influence of grain rotation on the structure of dust aggregates. Icarus 2006; 182: 274–280.

Sbrizzai F, Faraldi P, Soldati A. Appraisal of three-dimensional numerical simulation for sub-micron particle deposition in a micro-porous ceramic filter. Chemical Engineering Science 2005; 60: 6551–6563.

Sorensen CM. Light Scattering by Fractal Aggregates: A Review. Aerosol Science and Technology 2001; 35: 648–687.

Yamamoto K, Oohori S, Yamashita H, Daido S. Simulation on soot deposition and combustion in diesel particulate filter. Proceedings of the Combustion Institute 2009; 32: 1965–1972.

Figure captions

Figure 13 Fractal dimension of aggregates that grow in 20D × 20D × 80D, 30D × 30D × 80D, 40D × 40D × 80D, 60D × 60D × 80D, and 80D × 80D × 80D rectangular parallelepipeds. The error bars are shown only for the result of 473K.

Figure 1

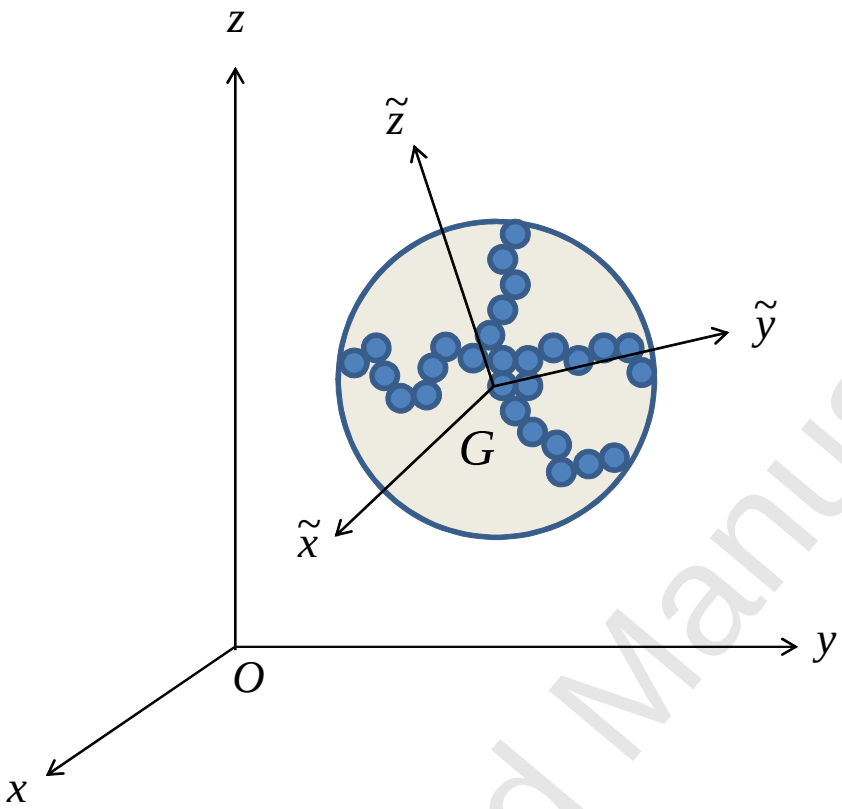

Figure 2

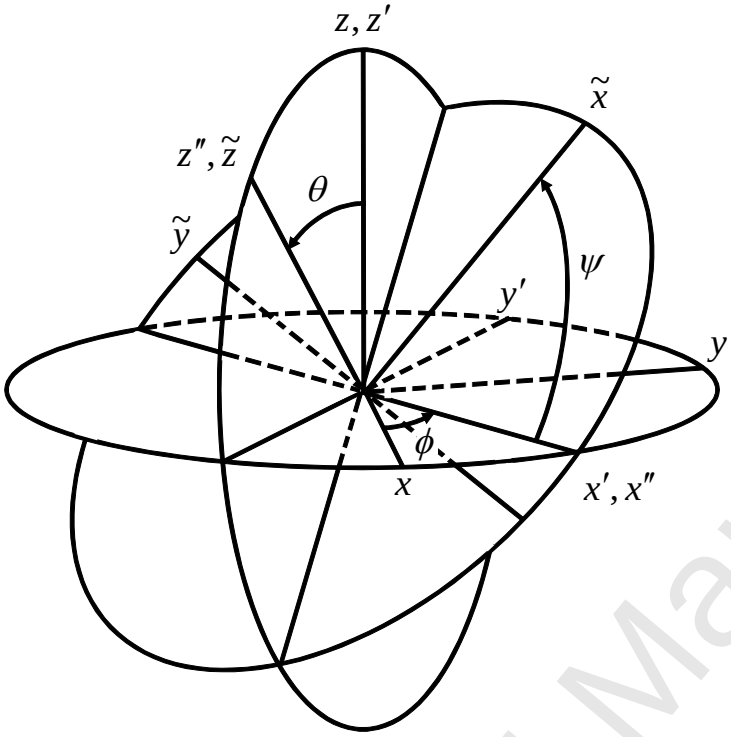

Figure 3

(a)

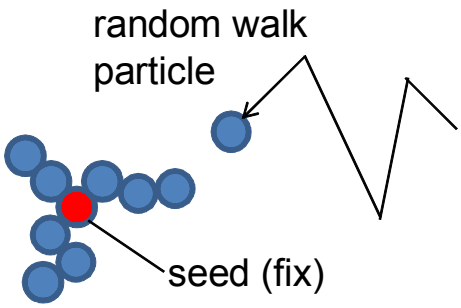

(b)

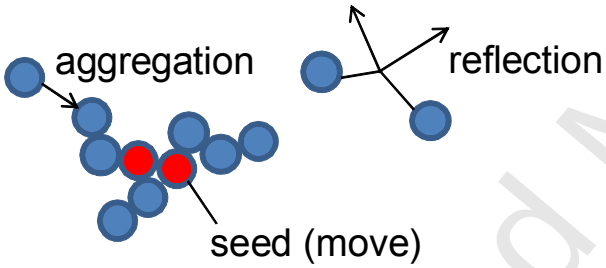

(c)

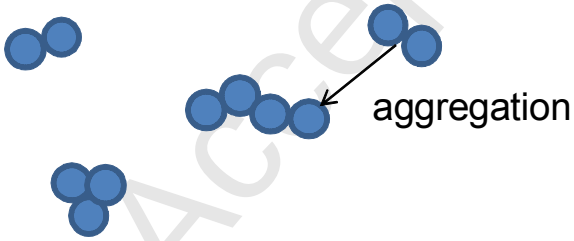

Figure 4

(a)

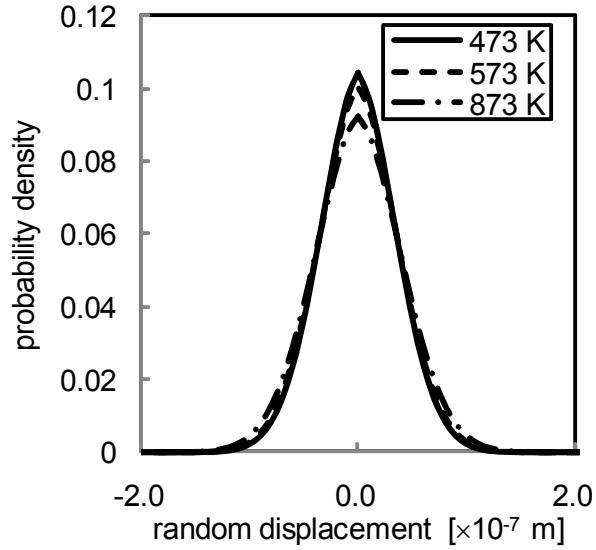

(b)

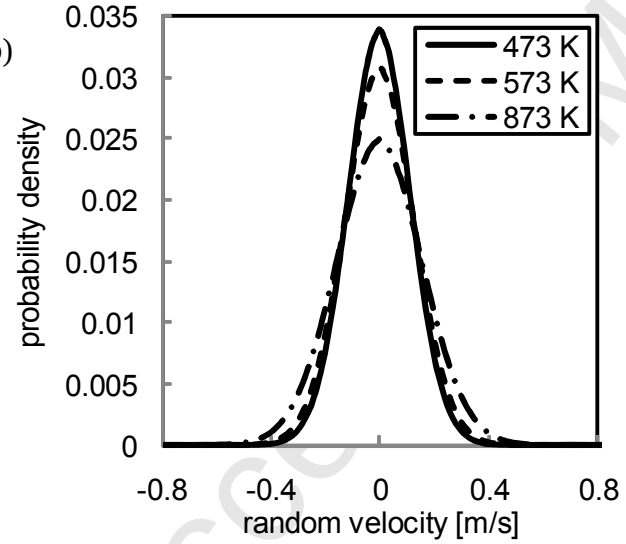

(c)

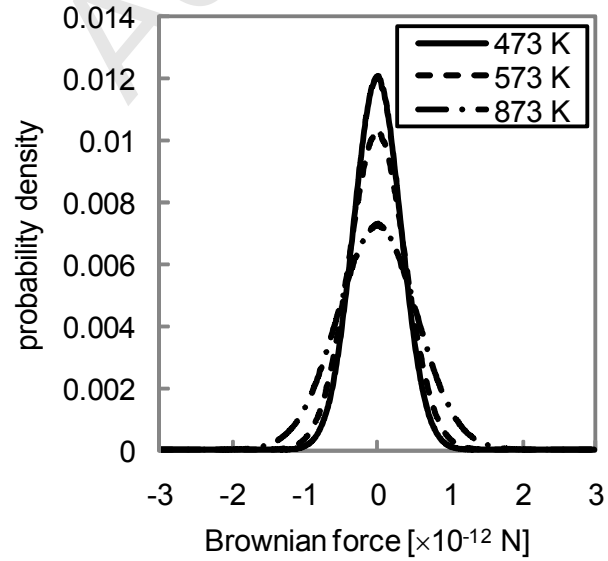

Figure 5

(a)

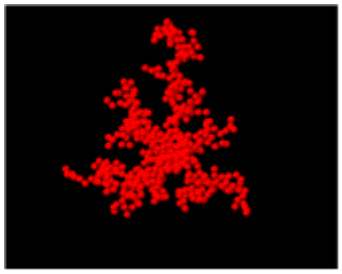

(b)

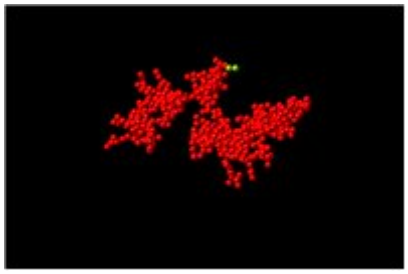

(c)

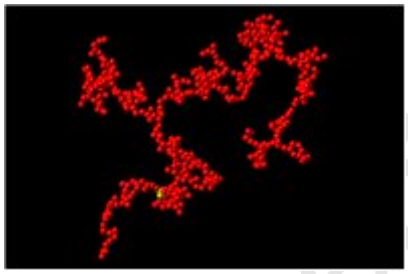

Figure 6

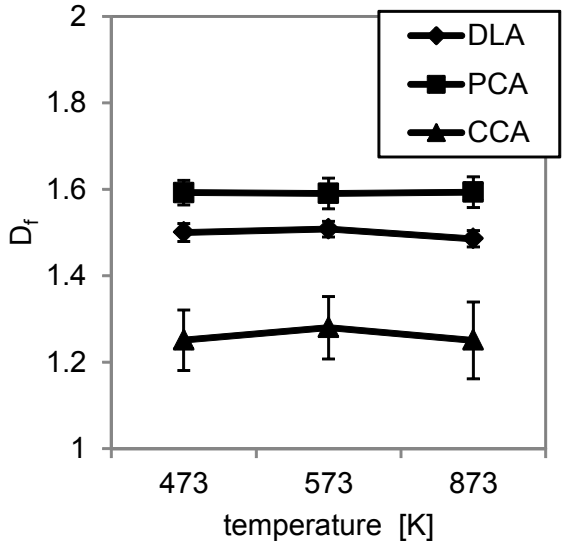

Figure 7

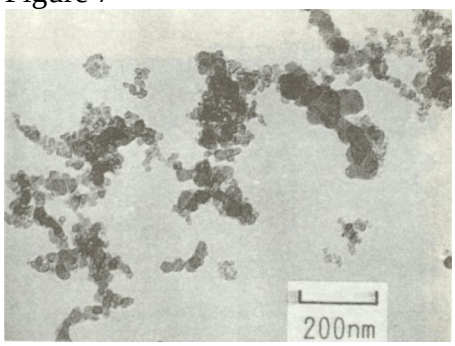

Figure 8

(a)

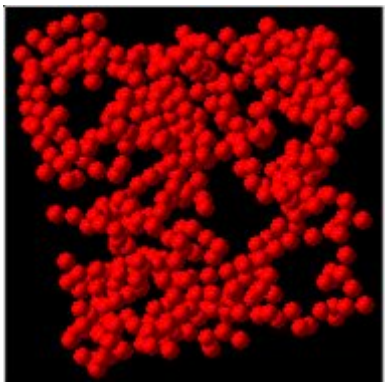

(b)

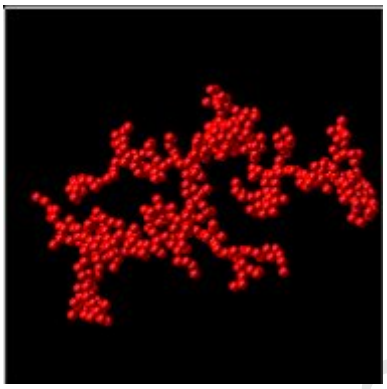

(c)

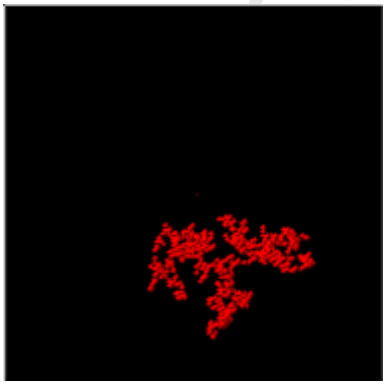

Figure 9

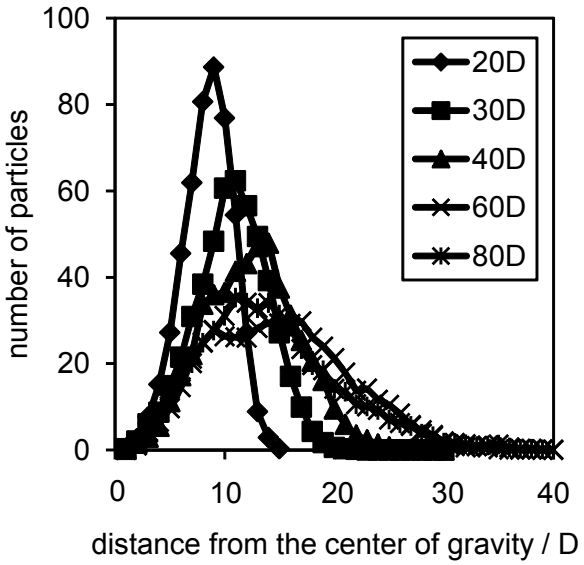

Figure 10

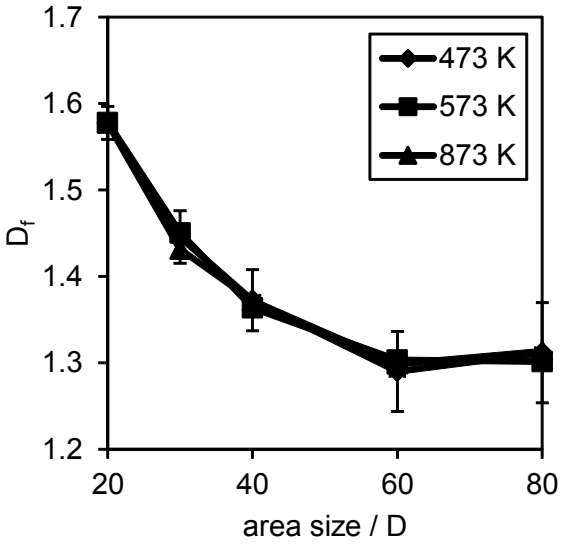

Figure 11

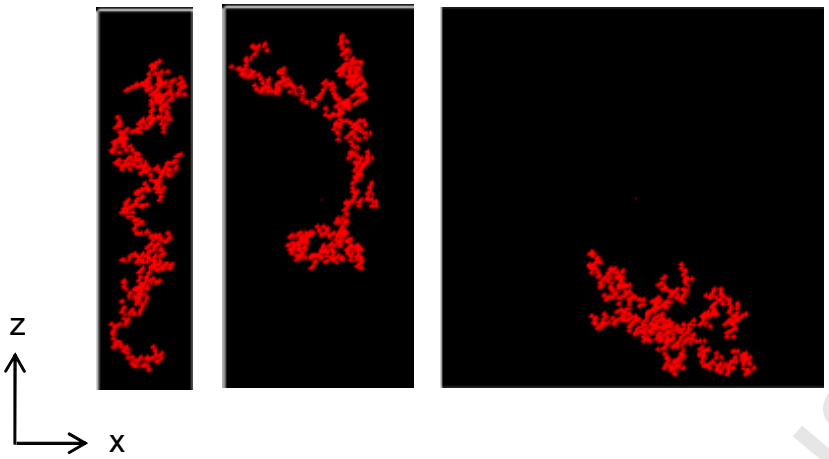

Figure 12

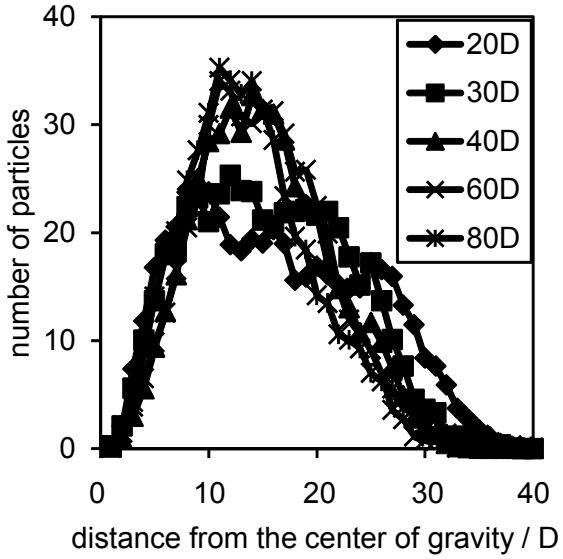

Figure 13

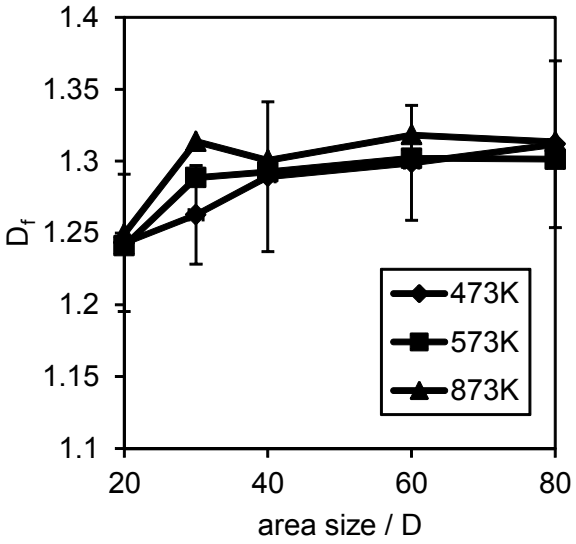

Highlights

The cluster−cluster aggregation model resulted in a soot-like branching shape. > Gas temperature affected the shielding effect of the aggregate branch. > The branching of the aggregate increased with low particle number density. > The size and aspect ratio of the field affected the aggregation shape.